THE JOURNAL OF PHYSICAL CHEMISTRY C

Article

pubs.acs.org/JPCC

High-Throughput Screening of Lead-Free Perovskite-like Materials for Optoelectronic Applications

Ankit Jain, Oleksandr Voznyy,* and Edward H. Sargent*

Department of Electrical and Computer Engineering, University of Toronto, 10 King's College Road, Toronto, Ontario M5S 3G4, Canada

Supporting Information

ABSTRACT: We use high-throughput density functional theory calculations to screen lead-free perovskite-like materials with compositions $A_2BB'X_6$, ABX_4, and $A_3B_2X_9$ for optoelectronic performance. We screen monovalent A and B′ cations from Na, K, Rb, Cs Cu, and Ag, trivalent B cations from Ga, In, and Sb, and monovalent anions from Cl, Br, and I. Our screening procedure is based on formation energy and hybrid HSE06 functional predicted bandgaps. We screened more than 480 compounds and found 10 compounds that have bandgaps in the 1.5−2.5 eV range. Of these 10 compounds, seven are new, not having been reported before. We further characterize effective masses, density of states, and absorption coefficients of these selected compounds for their suitability in optoelectronic applications. All 10 of these selected compounds are lead-free and are solution processable. These compounds pave a path forward for lead-free photovoltaics and light emission devices.

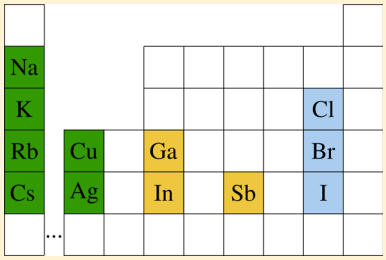

INTRODUCTION

Halide perovskites have attracted attention in recent years for their application in solar cells[1,2] and light-emitting devices.[3,4] The power conversion efficiency of perovskite-based solar cells is now becoming comparable to that of silicon photovoltaics.[5] Perovskites with bandgaps spanning near-infrared to visible wavelengths have been utilized in efficient light-emitting diodes and lasers.[6] Unfortunately, most of these high-performance perovskite materials are based on metals such as lead that are subject to environmental regulations.[7,8]

Researchers have implemented a partial or full substitution of lead metal with tin or germanium in the perovskite structure. These modified materials, however, have resulted in inferior device performance due to the unstable +2 oxidation state of tin and germanium.[9,10] Earlier predictions of new perovskite materials were based on the simple Goldschmidt tolerance factor to determine the stability of structure.[11] Recently, Travis et al.[12] showed that the Goldschmidt tolerance factor fails to predict the stability of 32 known inorganic iodide perovskites. Filip and Giustino[13] and Korbel et al.[14] performed high-throughput ab initio calculations on hypothetical three-dimensional halide perovskites (ABX_3) obtained by substitution of lead with other divalent cations from the periodic table. The authors considered hundreds of material combinations and concluded that only Pb, Sn, and Ge based perovskite show promising properties for optoelectronic applications.

Attempts have also been made to find perovskite-like structures via double perovskites, wherein two neighboring divalent lead cations are replaced by monovalent and trivalent ones.[15,16] Many other sister materials (such as $Cs_3Bi_2I_9$,[17] $AgBi_2I_7$,[18] and $Rb_3Sb_2I_9$[19]) are already synthesized and have shown promising photovoltaic power conversion efficiencies. These sister perovskite structures offer a broader search space and have only been partially explored for visible bandgap applications.

In this work, we use density functional theory (DFT) to conduct high-throughput screening of perovskite-like structures for their potential performance in photovoltaic and light-emitting devices. We considered four different structure types and more than 480 different materials. We screened the materials based on their stability and bandgaps from HSE06 functional calculations. We identify multiple halide-based materials that can be solution processed and have bandgaps in the visible range.

COMPUTATIONAL DETAILS

We employ a Perdew−Burke−Ernzerhof generalized gradient approximation (GGA) exchange-correlation functional[20] using the projected augmented wave pseudopotentials[21,22] as implemented in the computational package VASP[23] for all of our DFT calculations. Calculations are performed with plane-wave basis using a kinetic energy cutoff of 400 eV. For structural relaxation and formation energy calculations, the electronic wavevector grid is determined individually for each structure as $30/a$, where a is the length of the lattice vector (in Å) in the concerned direction.[a] The grid size is doubled for the calculation of bandgaps from DFT and HSE06 functional calculations.[24] For HSE06 Hartree−Fock/DFT hybrid functional calculations, we evaluate the Hartree−Fock contribution at the Gamma point only by setting the NKRED flag in the VASP INCAR file. We also performed HSE06 calculations with a denser wavevector grid for the final list of materials and found

Received: March 8, 2017
Revised: March 14, 2017
Published: March 16, 2017

DOI: 10.1021/acs.jpcc.7b02221
J. Phys. Chem. C XXXX, XXX, XXX−XXX

no change in the electronic bandgap. We relaxed all structures until the changes in total energies are less than 0.1 meV/atom.

While HSE06 functional results in better agreement with experiments, compared to GGA, it still does not fully describe the many-body effects. These effects can be included using GW or BSE calculations but are not considered in this work due to their high computational cost.

We note that spin−orbit interactions are not included in this work. Among studied materials, these interactions can be significant in Sb compounds.[16,25] We calculated the effect of spin−orbit coupling on our screened compounds and found changes in the GGA-predicted bandgaps to be less than 11% with the inclusion of spin−orbit interactions.

All the predictions are made using 0 K DFT relaxed structures and do not account for lattice expansion and temperature-induced phase changes due to high computational cost of entropic corrections. Such entropic corrections, however, are relatively small. Dispersion corrections are not included in this study as we focus on inorganic cations only. While van der Waals interactions could have significant effects on structural properties,[26] the effect is expected to be minimal for inorganic compounds considered in this work.

We calculated the density of states and absorption spectrum using HSE06 hybrid functional. For band structure and effective masses, we used GGA DFT calculations. All of the reported effective masses are conductivity effective masses[27] obtained as $m^* = 3/(1/m_1^* + 1/m_2^* + 1/m_3^*)$, where m_1^*, m_2^*, and m_3^* are effective masses in the (001), (010), and (100) directions, respectively.

SCREENING PROCEDURE

We present our screening procedure for identifying new materials in Figure S1. For a given structure type, we start by generating lattice structure and decorating lattice positions with anions and cations from the list of allowed species. We also generate a set of possible precursors, which a given material could decompose into, for the estimation of material stability. We calculate the electronic energies of the material and the precursors and use them to obtain the formation energy of the material relative to its precursors according to $FE = E_{material} - \sum E_{precursors}$, where $E_{material}$ and $E_{precursors}$ are the DFT predicted total energies of material and solid precursors. We note that even though this calculation of formation energy could result in false positives, it reliably eliminates all the negatives (i.e., unstable materials).

Having identified the subset of potentially stable materials, we calculate the bandgaps using a GGA functional and eliminate materials with gaps larger than 2.5 eV. Since GGA functional underpredicts the actual experimental bandgaps,[28] we next perform HSE06 functional calculations on selected materials and screen whether they have a direct bandgap in a range between 1.5 and 2.5 eV. Upon successful identification of potentially stable materials with bandgaps in the desired regime, we further calculate their effective masses, density of states, and absorption coefficients.

STRUCTURES

We start our search with literature investigation on solution processable materials. We find (nonexhaustive list) perovskite, double-perovskite,[25] vacancy-ordered double perovskite,[29] β-$GaBr_2$-type structures,[30] and two-dimensional perovskite (and its polymorph)[31] as potential lattice families. Of these, the perovskite family had been investigated in detail by Filip and Giustino[13] and Korbel et al.[14] using high-throughput calculations. Further, most of the literature reported compounds from vacancy-ordered double perovskite family are based on Sn metal,[29,32] which, similar to lead, has environmental concerns.[33] Therefore, we restricted our search to double perovskite, β-$GaBr_2$-type structures, and two-dimensional perovskite (and its polymorph) families.

The crystal structures of considered material families are presented in Figures 1a−d. These structures are discussed

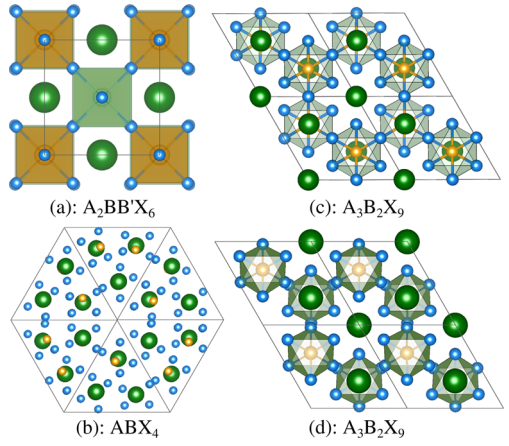

Figure 1. Different perovskite-like structures considered in this study with space groups (a) 87 ($I4/m$), (b) 161 ($R3c$), (c) 164 ($P\bar{3}m1$), and (d) 194 ($P6_3/mmc$). Structures (a), (c), and (d) are commonly referred as double, 2-D layered, and 0-D dimer perovskite, respectively. Structures (c) and (d) are polymorphs.

elsewhere.[30,31,34] These families belong to space groups 87 ($I4/m$), 161 ($R3c$), 164 ($P\bar{3}m1$), and 194 ($P6_3/mmc$) and have general chemical formulas $A_2BB'X_6$, ABX_4, $A_3B_2X_9$, and $A_3B_2X_9$ respectively, where A and B′ are monovalent cations, B is trivalent cation, and X is monovalent anion. Note that structure types (c) and (d) are polymorphs and structures (a), (c), and (d) are commonly referred to as double, 2-D layered, and 0-D dimer perovskites, respectively.

We considered 20, 36, 14, and 28 atom unit cells for structures (a), (b), (c), and (d), respectively, and restricted our search to pure phase materials only. Each of these structure types is composed of monovalent (A^+, B'^+) and trivalent (B^{3+}) cations and monovalent anions (X^-). We performed prescreening of ions on the basis of toxicity, solution processability, and feasibility of their large scale use in photovoltaic devices. Further, we restricted ourselves to inorganic ions.

A quick scan of stable favorable oxidation states of elements in the periodic table suggests alkali and coinage metals for monovalent cations. Of these, Au is expensive metal and is screened out. For trivalent cations, we restricted our search to p-block cations. From the possible list of Al^{3+}, Ga^{3+}, In^{3+}, Tl^{3+}, As^{3+}, Sb^{3+}, and Bi^{3+} cations, we removed Tl^{3+} and As^{3+} because of their toxicity. For anions, we focused on halides due of their solution processability. Finally, we remove small ions such as Al^{3+} and F^- from our list. We also removed Bi^{3+} because of additional computational cost associated with the spin−orbit coupling. The final list of cations and anions is presented in Figure 2. We select atoms from a list of 6 monovalent cations, 3 trivalent cations, and 3 monovalent anions.

DOI: 10.1021/acs.jpcc.7b02221
J. Phys. Chem. C XXXX, XXX, XXX−XXX

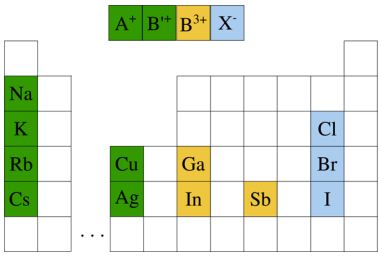

Figure 2. Periodic table with different monovalent cations, trivalent cations, and monovalent anions considered in this work.

RESULTS AND DISCUSSION

The above-described four crystal structures, along with all possible combinations of atoms, result in more than 480 total pure phase materials (formation energies and bandgaps of all of these compounds are reported in Table S1). Of these, around 3/4 are not stable and decompose into one or more precursors. Among the remaining materials, GGA band structure calculations eliminate around half of the materials with bandgaps larger than 2.5 eV. Finally, out of the remaining 65 compounds, hybrid HSE06 functional calculations predict 10 compounds to have direct bandgaps in the range of 1.5−2.5 eV (listed in Table 1).[b] We note that we found no material with bandgap less than 1.5 eV. We found 30 materials which have GGA-predicted bandgaps less than 2.5 eV and HSE06-predicted direct bandgap in the 2.5−3.5 eV range (see Supporting Information).

We find that with the exception of one compound, all copper based compounds resulted in a positive formation energy. For $Cu_3Ga_2Cl_9$ with space group 194 ($P6_3/mmc$), even though the formation energy is negative, its predicted bandgap from HSE06 is 3.98 eV.

We find that all of the compounds reported in Table 1 have bandgaps at the Γ-point (center) of the Brillouin zone. The smallest predicted bandgap is 1.72 eV for $Cs_3Ga_2I_9$. We find five compounds with bandgaps between 2.0 and 2.2 eV and four compounds with bandgaps between 2.3 and 2.5 eV. We note that while some of these compounds (such as $Rb_3Sb_2I_9$[19] and $Cs_3Sb_2I_9$[31]) have been studied before, most of these (such as $Cs_3In_2I_9$ and $Cs_3Ga_2I_9$) have never been reported.

Our predicted bandgap for $Cs_2AgInCl_6$ is 2.42 eV from HSE06 calculations and is in close agreement with the recent prediction (2.1−2.6 eV) of Volonakis et al.[16] For $Cs_3Sb_2I_9$ in space groups 164 ($P\bar{3}m1$) and 194 ($P6_3/mmc$), our predicted bandgaps are 2.13 eV (direct) and 2.53 eV (indirect) and match closely with the predictions of Saparov et al.[31] (2.05 eV direct and 2.40 eV indirect).

For $Rb_2AgInCl_6$ and $Cs_2AgInCl_6$, predicted bandgaps are in the 2.40−2.45 eV range. These bandgaps could be reduced by replacement of Cl with Br or I. However, we find pure phase Rb_2AgInI_6, $Rb_2AgInBr_6$, Cs_2AgInI_6, and $Cs_2AgInBr_6$ to be unstable and to decompose into binary precursors. The bandgaps could potentially be reduced by partial replacement of Cl with Br and I in mixed phases,[2,35] not considered here.

We also calculate conductivity effective masses for these compounds and report the numbers in Table 1. All compounds are predicted to have effective masses larger than 0.45 and 0.27 for holes and electrons, respectively. These effective masses are larger than those in methylammonium lead iodide perovskite ($MAPbI_3$) and silicon [(m_h^*, m_e^*) equals (0.29, 0.23) and (0.16, 0.19) for $MAPbI_3$[36] and Si,[37] respectively].

We next looked into the possibility of replacing inorganic A cation with organic monovalent cations such as methylammonium (MA) and formamidinium (FA) without altering the electronic bandgap. For this we calculate the site-projected density of states and present the results for one compound from each space group in Figure 3 (total density of states for all compounds are reported in Figure S2).

We find that both B′ and X atoms contribute toward the valence band maximum (VBM) in $Rb_2AgInCl_6$. In the remaining three space group compounds, the VBM states are dominated by X atoms. For all space groups, the conduction band minimum (CBM) includes the contribution from both B and X atoms. Interestingly, the contribution of A atoms toward VBM and CBM is minimal in all compounds and practically does not affect the bandgap (Table 1). Larger organic A cations could potentially provide an additional degree of freedom for tuning the bandgap through changes in the cage bond angles, accommodating for the cation size.[38]

We also calculated the energy-dependent dielectric constants and present the results for one compound from each space group type in Figure 4 (see Figure S3 for dielectric functions of all screened compounds). We report $\sqrt{\epsilon_r^2 + \epsilon_i^2} - \epsilon_r$ (which is directly related to the absorption coefficient of a material), where ϵ_r and ϵ_i are real and imaginary parts of the energy-dependent dielectric constant obtained under the independent

Table 1. Potentially Stable Compounds with Bandgaps in the 1.5−2.5 eV Range[a]

compound	space group	formation energy (meV/atom)	E_g^{DFT} (eV)	E_g^{HSE06} (eV)	m_h^*/m_e	m_e^*/m_e
$Rb_2AgInCl_6$	87 ($I4/m$)	−7	0.89	2.40	0.45[b]	0.27
$Cs_2AgInCl_6$	87 ($I4/m$)	−9	0.93	2.42	0.50[b]	0.28
$RbSbI_4$	161 ($R3c$)	−5	1.75	2.34	1.36	0.59
$CsSbI_4$	161 ($R3c$)	−19	1.77	2.34	1.45	0.62
$K_3Sb_2I_9$	164 ($P\bar{3}m1$)	−4	1.45	2.04	0.60	0.27
$Rb_3Sb_2I_9$	164 ($P\bar{3}m1$)	−42	1.49	2.07	0.64	0.28
$Cs_3Sb_2I_9$	164 ($P\bar{3}m1$)	−79	1.55	2.13	0.79	0.30
$Rb_3In_2I_9$	194 ($P6_3/mmc$)	−42	1.07	2.05	0.88	0.56
$Cs_3In_2I_9$	194 ($P6_3/mmc$)	−75	1.15	2.12	0.86	0.64
$Cs_3Ga_2I_9$	194 ($P6_3/mmc$)	−24	0.77	1.72	0.94[b]	0.66

[a]The stability of compounds is characterized by its formation energy with respect to binary precursors. E_g^{DFT} and E_g^{HSE06} represent bandgaps from DFT and HSE06 hybrid functional calculations. The conductivity effective masses for holes and electrons (m_h^*, m_e^*) are normalized by free electron mass (m_e) and are obtained from plain DFT band structures (see Figure S4 for band structures). [b]We did not include nondispersive band in the calculation of conductivity effective mass for this compound.

DOI: 10.1021/acs.jpcc.7b02221
J. Phys. Chem. C XXXX, XXX, XXX−XXX

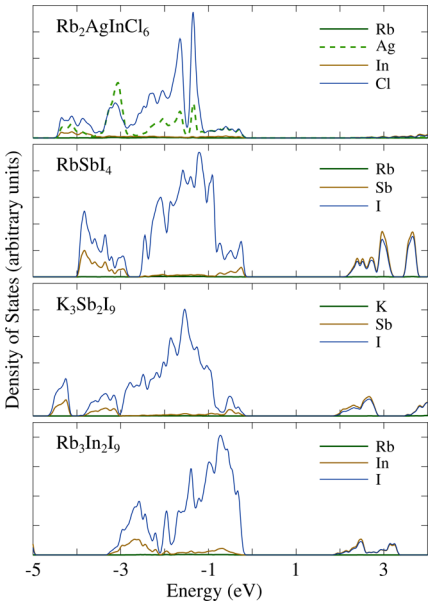

Figure 3. Site-projected density of states for $Rb_2AgInCl_6$, $RbSbI_4$, $K_3Sb_2I_9$, and $Rb_3In_2I_9$ obtained from HSE06 calculations. The minimal contribution of A cation toward the valence band maximum and conduction band minimum suggests a possibility of replacing the inorganic cation with an organic cation without significant changes in the electronic bandstructure. Energies are shifted to have Fermi level at 0 eV for all compounds.

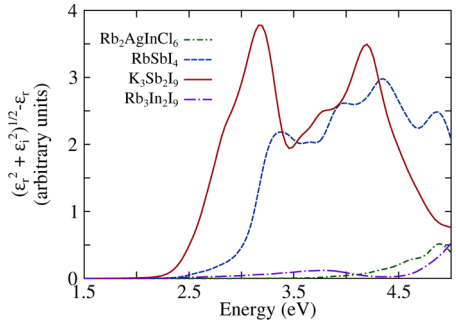

Figure 4. Energy-dependent dielectric functions of $Rb_2AgInCl_6$, $RbSbI_4$, $K_3Sb_2I_9$, and $Rb_3In_2I_9$ obtained from HSE06 calculations. ϵ_r and ϵ_i represents real and imaginary parts of the energy dependent dielectric constant.

particle approximation without considering local field effects[39] from HSE06 calculations.[c]

We find that due to a sparse density of conduction band edge states, the absorption coefficients are small in $Rb_2AgInCl_6$ and $Rb_3In_2I_9$. The absorption coefficients are highest for $K_3Sb_2I_9$, thereby suggesting stronger absorption in $K_3Sb_2I_9$ among considered compounds.

CONCLUSIONS

In summary, we used DFT calculations to screen materials from space groups 87 ($I4/m$), 161 ($R3c$), 164 ($P\bar{3}m1$), and 194 ($P6_3/mmc$) for visible bandgap applications. We screen materials on the basis of their stability and hybrid HSE06 functional predicted bandgaps.

We find 10 compounds which satisfy our screening criteria. The smallest bandgap in the visible range among studied compounds is predicted for $Cs_3Ga_2I_9$ (bandgap of 1.72 eV). We also present effective masses, density of states, and absorption coefficients for these screened compounds.

Our prediction of stable new materials with 1.5−2.5 eV bandgaps will help in advancing new materials research for optoelectronic devices. Efforts are currently in place to study bismuth structures and organic cation based and alloyed structures derived from the best structures obtained in this work.

ASSOCIATED CONTENT

Supporting Information

The Supporting Information is available free of charge on the ACS Publications website at DOI: 10.1021/acs.jpcc.7b02221.

Total density of states, dielectric functions, and bandgaps of screened compounds and formation energies and bandgaps of all compounds (PDF)

AUTHOR INFORMATION

Corresponding Authors

*E-mail o.voznyy@utoronto.ca; Tel 647-470-0092 (O.V.).

*E-mail ted.sargent@utoronto.ca; Tel 416-946-5051 (E.H.S.).

ORCID

Ankit Jain: 0000-0001-8091-9129

Oleksandr Voznyy: 0000-0002-8656-5074

Notes

The authors declare no competing financial interest.

ACKNOWLEDGMENTS

This research is supported in part by the Natural Sciences and Engineering Research Council (NSERC) of Canada, by the Ontario Research Fund Research Excellence Program, and by the IBM Canada Research and Development Center. A.J. is supported by the IBM Canada Research and Development Center through the Southern Ontario Smart Computing Innovation Platform (SOSCIP) postdoctoral fellowship. The SOSCIP consortium is funded by the Ontario Government and the Federal Economic Development Agency for Southern Ontario. Computations were performed on the GPC supercomputer at the SciNet HPC Consortium. SciNet is funded by the Canada Foundation for Innovation under the auspices of Compute Canada; the Government of Ontario; Ontario Research Fund - Research Excellence; and the University of Toronto. This work is partially funded by Samsung under the Global Research Outreach program. The authors thank B. Sutherland for his help with the manuscript preparation.

ADDITIONAL NOTES

[a]This correspond to wavevector grids of sizes 5 × 5 × 3, 2 × 2 × 2, 4 × 4 × 3, and 4 × 4 × 2 for space groups 87, 161, 164, and 194 with 20, 36, 14, and 28 atoms, respectively.

[b]Some of these compounds are found to have a slightly smaller indirect bandgap ($E_g^{indir} - E_g^{dir} < 0.03$, 0.09, 0.03, and 0.00 eV for space groups 87, 161, 164, and 194) but are treated as direct in this study.

[c]We find that ϵ_r and ϵ_i are direction dependent for some compounds, and we report only one direction for such compounds.

REFERENCES

(1) Green, M. A.; Ho-Baillie, A.; Snaith, H. J. The Emergence of Perovskite Solar Cells. *Nat. Photonics* **2014**, *8*, 506−514.

DOI: 10.1021/acs.jpcc.7b02221
J. Phys. Chem. C XXXX, XXX, XXX−XXX

(2) Stranks, S. D.; Snaith, H. J. Metal-Halide Perovskites for Photovoltaic and Light-Emitting Devices. *Nat. Nanotechnol.* **2015**, *10*, 391−402.
(3) Tan, Z.-K.; Moghaddam, R. S.; Lai, M. L.; Docampo, P.; Higler, R.; Deschler, F.; Price, M.; Sadhanala, A.; Pazos, L. M.; Credgington, D.; et al. Bright Light-Emitting Diodes Based on Organometal Halide Perovskite. *Nat. Nanotechnol.* **2014**, *9*, 687−692.
(4) Deschler, F.; Price, M.; Pathak, S.; Klintberg, L. E.; Jarausch, D.-D.; Higler, R.; Hüttner, S.; Leijtens, T.; Stranks, S. D.; Snaith, H. J.; et al. High Photoluminescence Efficiency and Optically Pumped Lasing in Solution-Processed Mixed Halide Perovskite Semiconductors. *J. Phys. Chem. Lett.* **2014**, *5*, 1421−1426.
(5) Saliba, M.; Matsui, T.; Domanski, K.; Seo, J.-Y.; Ummadisingu, A.; Zakeeruddin, S. M.; Correa-Baena, J.-P.; Tress, W. R.; Abate, A.; Hagfeldt, A.; et al. Incorporation of Rubidium Cations into Perovskite Solar Cells Improves Photovoltaic Performance. *Science* **2016**, *354*, 206−209.
(6) Xing, G.; Mathews, N.; Lim, S. S.; Yantara, N.; Liu, X.; Sabba, D.; Grätzel, M.; Mhaisalkar, S.; Sum, T. C. Low-Temperature Solution-Processed Wavelength-Tunable Perovskites for Lasing. *Nat. Mater.* **2014**, *13*, 476−480.
(7) Espinosa, N.; Serrano-Luján, L.; Urbina, A.; Krebs, F. C. Solution and Vapour Deposited Lead Perovskite Solar Cells: Ecotoxicity from a Life Cycle Assessment Perspective. *Sol. Energy Mater. Sol. Cells* **2015**, *137*, 303−310.
(8) Giustino, F.; Snaith, H. J. Toward Lead-Free Perovskite Solar Cells. *ACS Energy Lett.* **2016**, *1*, 1233−1240.
(9) Noel, N. K.; Stranks, S. D.; Abate, A.; Wehrenfennig, C.; Guarnera, S.; Haghighirad, A.-A.; Sadhanala, A.; Eperon, G. E.; Pathak, S. K.; Johnston, M. B.; et al. Lead-Free Organic-Inorganic Tin Halide Perovskites for Photovoltaic Applications. *Energy Environ. Sci.* **2014**, *7*, 3061−3068.
(10) Hao, F.; Stoumpos, C. C.; Cao, D. H.; Chang, R. P.; Kanatzidis, M. G. Lead-Free Solid-State Organic-Inorganic Halide Perovskite Solar Cells. *Nat. Photonics* **2014**, *8*, 489−494.
(11) Kieslich, G.; Sun, S.; Cheetham, A. K. An Extended Tolerance Factor Approach for Organic-Inorganic Perovskites. *Chem. Sci.* **2015**, *6*, 3430−3433.
(12) Travis, W.; Glover, E.; Bronstein, H.; Scanlon, D.; Palgrave, R. On the Application of the Tolerance Factor to Inorganic and Hybrid Halide Perovskites: A Revised System. *Chem. Sci.* **2016**, *7*, 4548−4556.
(13) Filip, M. R.; Giustino, F. Computational Screening of Homovalent Lead Substitution in Organic-Inorganic Halide Perovskites. *J. Phys. Chem. C* **2015**, *120*, 166−173.
(14) Körbel, S.; Marques, M. A.; Botti, S. Stability and Electronic Properties of New Inorganic Perovskites from High-Throughput Ab Initio Calculations. *J. Mater. Chem. C* **2016**, *4*, 3157−3167.
(15) McClure, E. T.; Ball, M. R.; Windl, W.; Woodward, P. M. Cs_2AgBiX_6 (X= Br, Cl): New Visible Light Absorbing, Lead-Free Halide Perovskite Semiconductors. *Chem. Mater.* **2016**, *28*, 1348−1354.
(16) Volonakis, G.; Haghighirad, A. A.; Milot, R. L.; Sio, W. H.; Filip, M. R.; Wenger, B.; Johnston, M. B.; Herz, L. M.; Snaith, H. J.; Giustino, F. $Cs_2InAgCl_6$: A New Lead-Free Halide Double Perovskite with Direct Band Gap. *J. Phys. Chem. Lett.* **2017**, *8*, 772−778.
(17) Park, B.-W.; Philippe, B.; Zhang, X.; Rensmo, H.; Boschloo, G.; Johansson, E. M. Bismuth Based Hybrid Perovskites $A_3Bi_2I_9$ (A: Methylammonium or Cesium) for Solar Cell Application. *Adv. Mater.* **2015**, *27*, 6806−6813.
(18) Kim, Y.; Yang, Z.; Jain, A.; Voznyy, O.; Kim, G.-H.; Liu, M.; Quan, L. N.; García de Arquer, F. P.; Comin, R.; Fan, J. Z.; et al. Pure Cubic-Phase Hybrid Iodobismuthates $AgBi_2I_7$ for Thin-Film Photovoltaics. *Angew. Chem., Int. Ed.* **2016**, *55*, 9586−9590.
(19) Harikesh, P.; Mulmudi, H. K.; Ghosh, B.; Goh, T. W.; Teng, Y. T.; Thirumal, K.; Lockrey, M.; Weber, K.; Koh, T. M.; Li, S.; et al. Rb as an Alternative Cation for Templating Inorganic Lead-Free Perovskites for Solution Processed Photovoltaics. *Chem. Mater.* **2016**, *28*, 7496−7504.
(20) Perdew, J. P.; Burke, K.; Ernzerhof, M. Generalized Gradient Approximation Made Simple. *Phys. Rev. Lett.* **1996**, *77*, 3865.
(21) Blöchl, P. E. Projector Augmented-Wave Method. *Phys. Rev. B: Condens. Matter Mater. Phys.* **1994**, *50*, 17953.
(22) Kresse, G.; Joubert, D. From Ultrasoft Pseudopotentials to the Projector Augmented-Wave Method. *Phys. Rev. B: Condens. Matter Mater. Phys.* **1999**, *59*, 1758.
(23) Kresse, G.; Hafner, J. Ab Initio Molecular Dynamics for Liquid Metals. *Phys. Rev. B: Condens. Matter Mater. Phys.* **1993**, *47*, 558.
(24) Krukau, A. V.; Vydrov, O. A.; Izmaylov, A. F.; Scuseria, G. E. Influence of the Exchange Screening Parameter on the Performance of Screened Hybrid Functionals. *J. Chem. Phys.* **2006**, *125*, 224106−224106.
(25) Volonakis, G.; Filip, M. R.; Haghighirad, A. A.; Sakai, N.; Wenger, B.; Snaith, H. J.; Giustino, F. Lead-Free Halide Double Perovskites via Heterovalent Substitution of Noble Metals. *J. Phys. Chem. Lett.* **2016**, *7*, 1254−1259.
(26) Wang, Y.; Gould, T.; Dobson, J. F.; Zhang, H.; Yang, H.; Yao, X.; Zhao, H. Density Functional Theory Analysis of Structural and Electronic Properties of Orthorhombic Perovskite $CH_3NH_3PbI_3$. *Phys. Chem. Chem. Phys.* **2013**, *16*, 1424−1429.
(27) He, Y.; Galli, G. Perovskites for Solar Thermoelectric Applications: A First Principle Study of $CH_3NH_3AI_3$ (A= Pb and Sn). *Chem. Mater.* **2014**, *26*, 5394−5400.
(28) Chan, M.; Ceder, G. Efficient Band Gap Prediction for Solids. *Phys. Rev. Lett.* **2010**, *105*, 196403.
(29) Lee, B.; Stoumpos, C. C.; Zhou, N.; Hao, F.; Malliakas, C.; Yeh, C.-Y.; Marks, T. J.; Kanatzidis, M. G.; Chang, R. P. Air-Stable Molecular Semiconducting Iodosalts for Solar Cell Applications: Cs_2SnI_6 as a Hole Conductor. *J. Am. Chem. Soc.* **2014**, *136*, 15379−15385.
(30) Burnus, R.; Meyer, G. Synthese und Kristallstrukturen der Alkali-Tetraiodoindate (III), $AlnI_4$ (A= Li, K, Rb, Cs). *Z. Anorg. Allg. Chem.* **1991**, *602*, 31−37.
(31) Saparov, B.; Hong, F.; Sun, J.-P.; Duan, H.-S.; Meng, W.; Cameron, S.; Hill, I. G.; Yan, Y.; Mitzi, D. B. Thin-Film Preparation and Characterization of $Cs_3Sb_2I_9$: A Lead-Free Layered Perovskite Semiconductor. *Chem. Mater.* **2015**, *27*, 5622−5632.
(32) Kaltzoglou, A.; Antoniadou, M.; Kontos, A. G.; Stoumpos, C. C.; Perganti, D.; Siranidi, E.; Raptis, V.; Trohidou, K.; Psycharis, V.; Kanatzidis, M. G.; et al. Optical-Vibrational Properties of the Cs_2SnX_6 (X= Cl, Br, I) Defect Perovskites and Hole-Transport Efficiency in Dye-Sensitized Solar Cells. *J. Phys. Chem. C* **2016**, *120*, 11777−11785.
(33) Babayigit, A.; Thanh, D. D.; Ethirajan, A.; Manca, J.; Muller, M.; Boyen, H.-G.; Conings, B. Assessing the Toxicity of Pb-and Sn-Based Perovskite Solar Cells in Model Organism Danio Rerio. *Sci. Rep.* **2016**, *6*, 18721.
(34) Filip, M. R.; Hillman, S.; Haghighirad, A. A.; Snaith, H. J.; Giustino, F. Band Gaps of the Lead-Free Halide Double Perovskites $Cs_2BiAgCl_6$ and $Cs_2BiAgBr_6$ from Theory and Experiment. *J. Phys. Chem. Lett.* **2016**, *7*, 2579−2585.
(35) Sutton, R. J.; Eperon, G. E.; Miranda, L.; Parrott, E. S.; Kamino, B. A.; Patel, J. B.; Hörantner, M. T.; Johnston, M. B.; Haghighirad, A. A.; Moore, D. T.; et al. Bandgap-Tunable Cesium Lead Halide Perovskites with High Thermal Stability for Efficient Solar Cells. *Adv. Energy Mater.* **2016**, *6*, 1502458−6.
(36) Giorgi, G.; Fujisawa, J.-I.; Segawa, H.; Yamashita, K. Small Photocarrier Effective Masses Featuring Ambipolar Transport in Methylammonium Lead Iodide Perovskite: A Density Functional Analysis. *J. Phys. Chem. Lett.* **2013**, *4*, 4213−4216.
(37) Gray, D. E. *American Institute of Physics Handbook*; McGraw-Hill: New York, 1982.
(38) Knutson, J. L.; Martin, J. D.; Mitzi, D. B. Tuning the Band Gap in Hybrid Tin Iodide Perovskite Semiconductors using Structural Templating. *Inorg. Chem.* **2005**, *44*, 4699−4705.
(39) Gajdoš, M.; Hummer, K.; Kresse, G.; Furthmüller, J.; Bechstedt, F. Linear Optical Properties in the Projector-Augmented Wave Methodology. *Phys. Rev. B: Condens. Matter Mater. Phys.* **2006**, *73*, 045112.

DOI: 10.1021/acs.jpcc.7b02221
J. Phys. Chem. C XXXX, XXX, XXX−XXX